American Mineralogist, Volume 108, pages 59–69, 2023

Oxidation or cation re-arrangement? Distinct behavior of riebeckite at high temperature

Giancarlo Della Ventura[1,2,3,*], Günther J. Redhammer[4], Federico Galdenzi[1,2], Gennaro Ventruti[5], Umberto Susta[1], Roberta Oberti[6], Francesco Radica[1,2], and Augusto Marcelli[2,7]

[1]Dipartimento di Scienze, Università di Roma Tre, L.S. Leonardo Murialdo 1, 00146 Rome, Italy
[2]INFN-LNF, Via E. Fermi 40, Frascati 00044 Rome, Italy
[3]INGV, Via di Vigna Murata 605, 00143 Rome, Italy
[4]Department Chemistry Physics of Materials, University of Salzburg, Jakob-Haringerstr. 2A, 5020 Salzburg, Austria
[5]Dipartimento di Scienze della Terra e Geoambientali, University of Bari, Via Orabona 4, 70125 Bari, Italy
[6]CNR-Istituto di Geoscienze e Georisorse, sede secondaria di Pavia, via Ferrata 1, I-27100 Pavia, Italy
[7]Rome International Centre for Material Science Superstripes—RICMASS, Via dei Sabelli 119A, 00185 Rome, Italy

Abstract

In this work we address the stability of riebeckite at high temperatures and compare the different behaviors observed under various oxidation conditions. For this purpose, we annealed powders of a sample from Mt. Malosa (Malawi), which is compositionally close to the end-member; the run products obtained after annealing in air vs. in vacuum were studied by Mössbauer spectroscopy and powder X-ray diffraction. The results show that riebeckite follows two distinct paths depending on the external environment. Under oxidizing conditions, it is stable in the hydrous form up to relatively low temperatures (400–450 °C), then it undergoes a rapid (within ~50 °C) dehydrogenation, forming oxo-riebeckite, which is stable up to ~900 °C. The final breakdown products of the oxo-amphibole include aegirine + cristobalite + hematite. Based on the relative intensity of the (310) Bragg reflection, the activation energy (E_a) for the riebeckite to oxo-riebeckite transition is 166 ± 6 kJ/mol.

Under vacuum conditions, no Fe oxidation is observed, and riebeckite is stable up to much higher temperatures (750–800 °C); however, in the $550 < T < 700$ °C range, it undergoes a significant re-arrangement of the C cations (those hosted in the strip of octahedra). Indeed, the amphibole stable in the 700–800 °C range has the same chemical formula as riebeckite but has a disordered and non-standard cation distribution at the octahedra, i.e., $^{M(1)}(Fe^{3+}Fe^{2+})^{M(2)}(Fe^{3+}Fe^{2+})^{M(3)}Fe^{2+}$; we call this phase "$^{C}R^{3+}$ disordered riebeckite". For $T \geq 800$ °C, it decomposes to aegirine + fayalite + cristobalite + H_2O.

External oxygen is required for the release of water into the surrounding system, being a prerequisite for the Fe-amphiboles to be a carrier of H_2O in the lower crust and upper mantle. One important implication of our results is that characterization of the overall oxidation state of iron does not necessarily provide the redox conditions of the environment of formation because a crystal-chemical re-arrangement under reducing conditions allows riebeckite to maintain its Fe^{3+}/Fe^{2+} composition up to higher temperatures.

Keywords: riebeckite, HT experiments, vacuum conditions, Mössbauer spectroscopy, X-ray powder diffraction

Introduction

Riebeckite, ideally $Na_2(Fe^{2+}_3Fe^{3+}_2)Si_8O_{22}(OH)_2$, is a relatively common iron-rich member of the sodic amphibole subgroup; it is typically found in acid igneous rocks and as an important constituent of high-grade shists and meta-iron stones (Deer et al. 1997). The phase relations of riebeckite in the system Na_2O-FeO-SiO_2-H_2O under hydrothermal conditions have been experimentally determined by Ernst (1962, 1968) at varying oxygen fugacity, temperature, and pressure. According to these studies, end-member riebeckite is stable below ~500 °C, 1000 bars at an f_{O_2} defined by the hematite-magnetite buffer; the effect of pressure was found to be rather limited with the stability increasing to ~600 °C at 2 kbar. The breakdown product included hematite + magnetite + quartz + acmite + fluid (Ernst 1962). Under more reducing conditions (magnetite-quartz-fayalite buffer), the stability of the amphibole increases to ~700 °C at 1 kbar. The fibrous form of riebeckite is the asbestos mineral known as "crocidolite." Several studies on the thermal stability of crocidolite were done mostly in the 1960s and 1970s (see Della Ventura et al. 2018, 2021 for a complete list of references) mainly because crocidolite was used for efficient fire-resistant textiles. These studies were focused on the products of decomposition of crocidolite as a function of temperature, both in air and under an inert (Ar, N_2) atmosphere. In particular, Hodgson et al. (1965) and Whitfield and Freeman (1967) observed the appearance, at

* E-mail: giancarlo.dellaventura@uniroma3.it. Orcid 0000-0001-6277-961X

500–600 °C in N_2 atmosphere, of a modified amphibole phase named "crocidolite anhydrite"; the structural details of this phase were not determined. Under oxidizing conditions, the formation of "oxycrocidolite" was observed at 300–450 °C by Whitfield and Freeman (1967). The amphibole transformations under reducing conditions were also investigated by Addison and Sharp (1962), as well as the kinetics of H diffusion (Addison et al. 1962; Clark and Freeman 1967). The oxidation dynamics of iron in riebeckite during thermal annealing in air have been studied in detail by using a multi-methodological approach combining single-crystal structure refinement (SREF) with FTIR, Raman, XAS, and Mössbauer spectroscopy (Oberti et al. 2018; Della Ventura et al. 2018, 2021; Galdenzi et al. 2018); the process can be described by the simple reaction:

$$^{M(1)}Fe^{2+} + {}^{O(3)}OH^{-} \rightarrow {}^{M(1)}Fe^{3+} + {}^{O(3)}O^{2-} + \tfrac{1}{2}H2 \quad (1)$$

whereby ferrous iron at the *M*(1) site is oxidized to ferric iron, the local charge balance is maintained by the loss of H^+ ions at the anionic O(3) site (Oberti et al. 2018). However, Della Ventura et al. (2018) showed that Fe-oxidation in riebeckite is indeed a much more complex process that depends strongly on the thermal range: (1) up to 450 °C, Fe oxidation is reversible; in the Raman spectra collected in situ during the annealing experiments the O-H stretching signal disappears, and peaks assigned to Fe^{3+}-O modes appear. However, when the sample is quenched at room temperature, the O-H signal is recovered, and the ferric iron reduces to ferrous iron. We must conclude that in this *T* range, both electrons (e^-) and hydrogen cations (H^+) are delocalized but remain within the amphibole matrix. (2) In the *T* interval 450–550 °C, all ferrous iron irreversibly oxidizes to ferric iron, as indicated by Mössbauer spectroscopy and by the definitive collapse of the unit-cell parameters (Oberti et al. 2018; Della Ventura et al. 2018). Raman spectroscopy was done on cooling and also showed irreversible modifications of the lattice modes and the final disappearance of the O-H stretching signal. Therefore, the thermal energy supplied to the system is high enough for the expulsion of both the electrons and the protons from the structure. However, FTIR spectra collected in transmission through the crystal still show the presence of residual OH in the matrix core, implying that dehydrogenation starts at the surface of the sample, triggered by the presence of external oxygen. (3) At $T > 550$ °C, FTIR spectroscopy is coherent with the total loss of H^+, and thus with complete Fe oxidation. This process is irreversible, and the resulting oxo-amphibole is stable up to ~900 °C (Oberti et al. 2018). The reversible oxidation of iron up to 450 °C had never been observed so far for other minerals and might have an important bearing in several other disciplines, including geophysics, toxicology, and technology. It is worth noting that a similar behavior has recently been observed also in grunerite, ideally $Fe_7^{2+}Si_8O_{22}(OH)_2$ (Mihailova et al. 2021).

The work described here was done to gain further insight into the oxidation of iron by direct measurement of its valence state via Mössbauer spectroscopy on samples annealed at different temperatures and different redox conditions. The spectroscopic data were augmented by powder X-ray diffraction to follow the structural adjustments and identify the decomposition products with increasing *T*.

Experimental methods

The studied powders were obtained from centimeter-sized, pegmatitic riebeckite crystals from Mt. Malosa, Zomba District (Malawi), described by Susta et al. (2018); the crystal-chemistry of the amphibole was fully characterized by using a combination of methods, including SREF, EMP, LA-ICPMS, FTIR, Raman, and Mössbauer spectroscopies (Oberti et al. 2018; Della Ventura et al. 2018). The resulting composition is very close to that of the end-member $^{A}\square{}^{B}Na_2{}^{C}(Fe_3^{2+}Fe_2^{3+})$ $^{T}Si_8O^{W}_{22}(OH)_2$ (Oberti et al. 2018), the solid-solution observed implying small amounts of ^{C}Mg (0.26 apfu) and ^{B}Ca (0.13 apfu), plus negligible ^{C,T}Al (0.11 apfu in total), ^{C}Ti (0.01 apfu), and ^{W}F (0.1 apfu).

Mössbauer spectra were collected at the University of Salzburg (Austria). Annealing was done in fused silica glass cells under dynamic high vacuum (HV) and slow evacuation down to $<9 \times 10^{-6}$ mbar. After HV was reached, the temperature was increased at a rate of 10 °C/min to avoid strong particle movements, and the sample was kept for 8 h at the target *T*, during which the pressure was continuously monitored; it was always lower than 10^{-6} mbar and around 10^{-7} after the experiment. Finally, the cell was extracted from the furnace while under a dynamic vacuum and allowed to cool to room temperature. Transmission ^{57}Fe Mössbauer data were collected in the air using an apparatus in a horizontal arrangement (^{57}Fe Co/Rh single-line thin source, constant acceleration mode with symmetric triangular velocity shape, a multi-channel analyzer with 1024 channels, regular velocity calibration against metallic Fe). Additional analyses were done using the same experimental apparatus on powders annealed in air at 450, 700, and 800 °C for 8 h. The spectra were evaluated using the RECOIL program suite (Rancourt and Ping 1991; Rancourt et al. 1993, 1996); patterns were corrected for thickness effects and then processed using the full static hyperfine interaction Hamiltonian analysis with Lorentzian-shaped doublets.

X-ray powder diffraction (XPRD) data were collected on the same annealed samples analyzed by Mössbauer spectroscopy using a Bruker D8 system (Ni-filtered Cu*K*α radiation, 0.3° divergence slits, 2.5° primary and secondary Soller slits, 1° anti-scatter slit) in combination with a Lynxeye detection system. Phase analysis was done using the EVA software package; quantitative phase analysis based on the Rietveld method was done using TOPAS V6.

In situ HT X-ray powder diffraction patterns were collected in the 2θ range 8–75° with steps of 0.013° at the Geology Department of the University of Bari, with an Empyrean PANalytical diffractometer operating in Bragg-Brentano geometry and equipped with a high-temperature (HT) cell (Anton Paar, model HTK 1200 N) using Ni-filtered, Cu*K*α radiation, and a PIXcel linear detector. The sample was heated from room temperature (RT) to 800 °C and then cooled back to RT, always using a 10 °C/min rate. Patterns were collected at RT, 100, and 200 °C, every 25 °C from 250 to 500 °C, at 550, 600, 700, and 800 °C, and then every 100 °C during cooling. The entire experiment lasted ~35 h. Whole-pattern data were refined by the Le Bail method using the General Structure Analysis System software (Larson and Von Dreele 2000).

Three sets of isothermal heating experiments were done in air at 400, 425, and 450 °C to study the riebeckite–oxo-riebeckite transition kinetics. Finely crushed riebeckite powder was transferred in a pre-heated Nabertherm furnace, and the temperature was held for different durations, from 0.5 to 24 h. At the end of the experiment, the powder was extracted from the furnace and cooled in air, and then analyzed via XRPD.

Experimental results

Heating in vacuum: Mössbauer spectroscopy

Selected refined ^{57}Fe Mössbauer spectra are shown in Figure 1, and all collected spectra can be found in the Online Materials[1] Fig. S1; refined parameters are listed in Table 1. The RT spectrum of riebeckite was already described in Susta et al. (2018) and Oberti et al. (2018). It shows four well-separated resonance absorption lines with two additional shoulders and can be satisfactorily fit using three doublets corresponding to Fe^{2+} at the *M*(1) and *M*(3) sites and to Fe^{3+} at the *M*(2) site, respectively. All spectral features can be perfectly matched with this three-doublet fit. Hence, there is no evidence for Fe^{2+} at *M*(2), which is mainly occupied by Fe^{3+}. Also, there is no evidence for Fe^{2+} at the *M*(4) site. Upon annealing in vacuum and ex-situ analysis, no change in the spectra is observed up to 500 °C (Table 1).

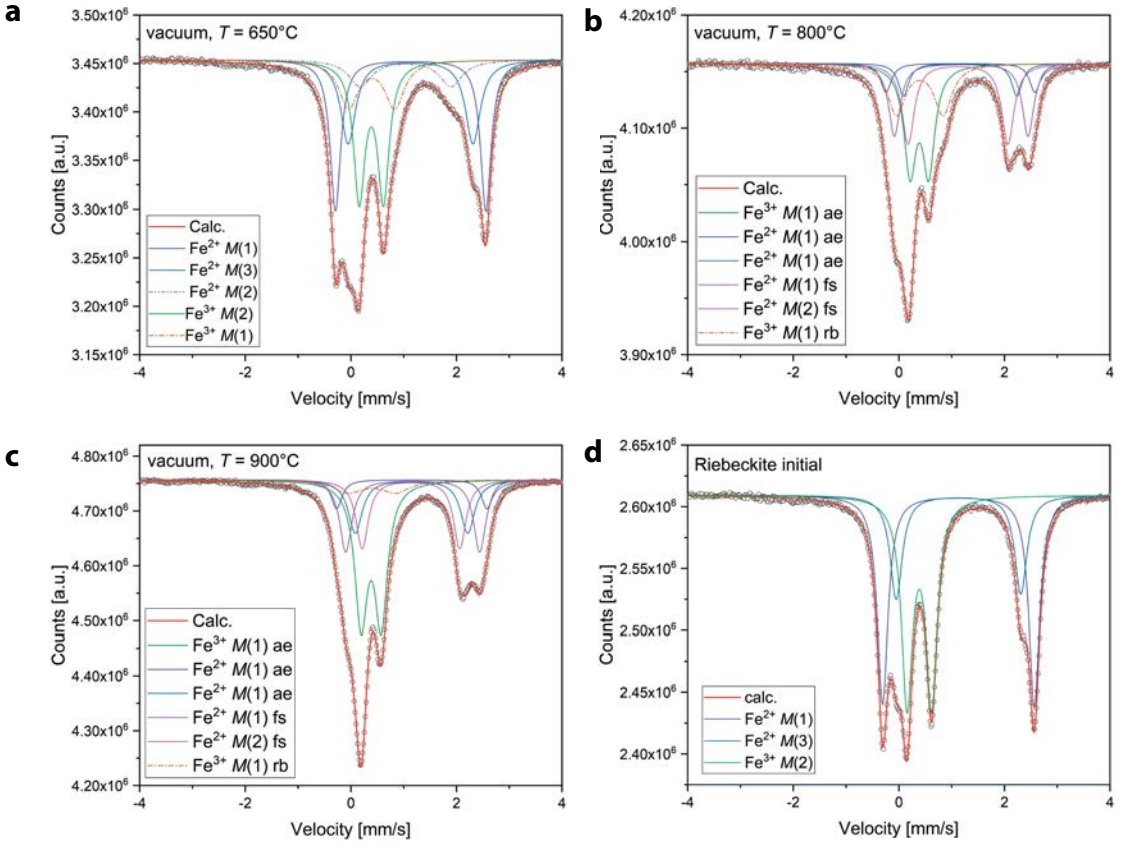

Figure 1. Selected fitted Mössbauer spectra after annealing the sample in vacuum at different temperatures. ae = aegirine, fs = ferrosilite, rb = riebeckite. (Color online.)

At 550 °C, very small shoulders appear at ~1 and ~1.8 mm/s. They are too weak to be fitted, but their positions suggest that at least two new doublets are now required to model the pattern. Hence, in the sample annealed at 600 °C, two additional doublets were introduced. Based on their isomer shifts, they can be assigned to ferrous and ferric iron in octahedral coordination, respectively. The doublet assigned to Fe^{3+} has a larger quadrupole splitting (QS) than that assigned to Fe^{3+} at *M*(2), while the doublet assigned to Fe^{2+} has a smaller QS than that assigned to Fe^{2+} at *M*(1); both features are indicative of more distorted local environments around the Fe probe nuclei (Della Ventura et al. 2016). These new spectral features are still weak in the sample annealed at 600 °C but become much more intense in the samples annealed at 650 and 700 °C (Fig. 1).

A visual representation of the data from Table 1 (Fig. 2) shows that annealing under vacuum does not produce any variation in the relative Fe^{3+}/Fe^{2+} site distribution up to 550 °C. In the 550 °C < *T* < 700 °C range, the fraction of $^{M(3)}Fe^{2+}$ remains constant at around 20% of total iron, and that of Fe^{3+}_{tot} only slightly increases above 40%; the amounts of $^{M(1)}Fe^{2+}$ and $^{M(2)}Fe^{3+}$ decrease significantly. We conclude that very limited Fe oxidation is accompanied by a significant cation exchange: $^{M(1)}Fe^{2+}$ migrates to *M*(2), and the same amount of $^{M(2)}Fe^{3+}$ migrates to *M*(1). Because the relative intensities of the two new doublets are almost equal, and their increase fits well the decrease of $^{M(2)}Fe^{3+}$ and $^{M(1)}Fe^{2+}$, we assign the two new doublets appearing during thermal annealing under vacuum to $^{M(2)}Fe^{2+}$ and $^{M(1)}Fe^{3+}$, respectively (Table 1). In summary, in the 550 < *T* < 700 °C range the Fe^{3+}/Fe^{2+} ratio in the amphibole remains almost constant, but the site partitioning of ^{C}Fe changes from $^{M(1)}Fe^{2+}_2{}^{M(2)}Fe^{3+}_2{}^{M(3)}Fe^{2+}$ to $^{M(1)}(Fe^{3+}Fe^{2+})\,^{M(2)}(Fe^{3+}Fe^{2+})^{M(3)}Fe^{2+}$, ferric iron being equally disordered over *M*(1) and *M*(2). According to the rules in force (Hawthorne et al. 2012), the name of the amphibole depends on the overall composition at the various group sites, and hence the products must still be named "riebeckite." However, the cation distribution is non-standard [Fe^{3+} strongly orders at *M*(2) in amphiboles in the absence of the oxo-component, see Hawthorne and Oberti (2007)]; therefore, we will name this phase "$^{C}R^{3+}$ disordered riebeckite" in the following.

An important point to consider here is that provided there is no Fe^{3+} short-range ordering at *M*(1), all local arrangements close to the hydroxyl group in $^{C}R^{3+}$ disordered riebeckite are still of the type $^{M(1)}Fe^{2+}_2{}^{M(1)}Fe^{2+}_2{}^{M(3)}Fe^{2+}$-OH (see Fig. 3). This being the case, there is no need for a loss of protons. In fact, 0.17 extra valence units converging on the hydroxyl oxygen O(3) can be easily accommodated by bond-length adjustments. The same feature is observed in pargasite, where trivalent cations such as Al may distribute between the *M*(2) and the *M*(3) sites in Mg-rich samples (Oberti et al. 1995; Della Ventura et al. 1999, 2003; Hawthorne and Della Ventura 2007). Actually, IR spectroscopy shows no OH loss in riebeckite powders heated at HT in an inert atmosphere, even for a prolonged time (Della Ventura et al. 2018, 2021).

Table 1. Fitted ^{57}Fe Mössbauer parameters for the riebeckite powders annealed in vacuum

Sample ID	IS δ mm/s	QS Δ mm/s	HWHM Γ/2 mm/s	A (%)	Assignment
25 °C initial	1.129(5)	2.874(2)	0.122(5)	39.0(6)	Fe^{2+} *M*(1)
	1.130(7)	2.361(5)	0.139(4)	21.5(7)	Fe^{2+} *M*(3)
	0.388(4)	0.465(2)	0.127(4)	39.5(3)	Fe^{3+} *M*(2)
450 °C	1.129(6)	2.871(3)	0.120(5)	38.7(7)	Fe^{2+} *M*(1)
	1.131(5)	2.360(3)	0.125(4)	22.4(6)	Fe^{2+} *M*(3)
	0.395(5)	0.456(4)	0.125(6)	38.9(4)	Fe^{3+} *M*(2)
500 °C	1.130(4)	2.866(4)	0.122(5)	38.0(6)	Fe^{2+} *M*(1)
	1.127(5)	2.365(3)	0.153(4)	23.0(7)	Fe^{2+} *M*(3)
	0.393(4)	0.463(3)	0.127(5)	39.0(4)	Fe^{3+} *M*(2)
550 °C	1.131(5)	2.860(4)	0.125(4)	38.2(7)	Fe^{2+} *M*(1)
	1.124(6)	2.350(6)	0.149(6)	21.7(7)	Fe^{2+} *M*(3)
	0.393(4)	0.467(4)	0.134(5)	40.2(5)	Fe^{3+} *M*(2)
600 °C	1.132(4)	2.859(5)	0.120(5)	31.8(8)	Fe^{2+} *M*(1)
	1.125(5)	2.367(4)	0.147(6)	20.2(7)	Fe^{2+} *M*(3)
	0.391(5)	0.465(4)	0.137(5)	35.4(4)	Fe^{3+} *M*(2)
	0.457(4)	0.829(6)	0.218(6)	6.1(9)	Fe^{3+} *M*(1)
	0.943(5)	1.93(7)	0.275(6)	6.5(9)	Fe^{2+} *M*(2)
650 °C	1.132(5)	2.849(6)	0.121(5)	26.9(7)	Fe^{2+} *M*(1)
	1.131(6)	2.364(6)	0.171(6)	21.2(7)	Fe^{2+} *M*(3)
	0.388(6)	0.458(4)	0.131(7)	26.4(5)	Fe^{3+} *M*(2)
	0.393(5)	0.873(6)	0.220(7)	15.3(8)	Fe^{3+} *M*(1)
	1.037(6)	1.719(6)	0.262(6)	10.3(9)	Fe^{2+} *M*(2)
700 °C	1.136(5)	2.843(7)	0.120(6)	21.3(6)	Fe^{2+} *M*(1)
	1.134(6)	2.371(6)	0.172(5)	18.2(7)	Fe^{2+} *M*(3)
	0.385(6)	0.487(5)	0.141(5)	23.0(5)	Fe^{3+} *M*(2)
	0.407(5)	0.915(6)	0.176(6)	18.7(8)	Fe^{3+} *M*(1)
	1.077(6)	1.767(8)	0.281(5)	18.8(8)	Fe^{2+} *M*(2)
800 °C	0.389(7)	0.353(2)	0.138(6)	27.3(9)	Fe^{3+} M1 (ae)
	1.167(8)	2.820(4)	0.121(3)	6.7(1.8)	Fe^{2+} M1 (ae)
	1.161(11)	2.147(4)	0.120(6)	7.4(1.9)	Fe^{2+} M1 (ae)
	1.182(7)	2.532(3)	0.131(3)	18.1(8)	Fe^{2+} M1 (fs)
	1.120(13)	1.890(6)	0.141(4)	21.5(9)	Fe^{2+} M2 (fs)
	0.396(15)	0.884(8)	0.200(5)	19.1(1.0)	Fe^{3+} *M*(1)
900 °C	0.384(6)	0.380(4)	0.144(6)	35.6(9)	Fe^{3+} M1 (ae)
	1.154(6)	2.848(5)	0.121(3)	6.3(9)	Fe^{2+} M1 (ae)
	1.148(6)	2.130(3)	0.160(3)	15.4(9)	Fe^{2+} M1 (ae)
	1.173(5)	2.537(4)	0.139(3)	18.0(6)	Fe^{2+} M1 (fs)
	1.139(5)	1.849(4)	0.149(4)	17.3(7)	Fe^{2+} M2 (fs)
	0.399(6)	0.899(3)	0.337(12)	7.3(8)	Fe^{3+} *M*(1)

Note: IS = isomer shift; QS = quadrupole splitting; HWHM = half-width at half maximum (peak width); A = relative fraction of total iron; ae = aegirine; fs = ferrosilite.

X-ray diffraction (see below) shows that the sample annealed at 800 °C consists of minor residual riebeckite (~20%) and large amounts of clinopyroxene [aegirine ($NaFe^{3+}Si_2O_6$) and ferrosilite ($Fe_2^{2+}Si_2O_6$)]. As deduced from lattice parameters, the aegirine probably contains some Ca, and thus an equal amount of Fe^{2+}, a suggestion that is also supported by the Mössbauer refinement (Table 1). In fact, the spectrum collected after annealing at 800 °C can only be evaluated by using two doublets for Fe^{2+} at the M1 and M2 sites in ferrosilite, and three doublets (one for Fe^{3+} and two for Fe^{2+}) in aegirine, which are typical for pyroxenes along the hedenbergite–aegirine join (Redhammer et al. 2006). A weak Fe^{3+} component is also required, which has Mössbauer parameters similar to those of the additional Fe^{3+} component [$^{M(1)}Fe^{3+}$] in the amphibole, and which should be assigned to riebeckite. Due to the large overlap, however, there is no clear evidence for the additional Fe^{2+} component [$^{M(2)}Fe^{2+}$] to be assigned to riebeckite. For the ferrosilite phase, the two doublets have almost equal area fractions (as expected from stoichiometry), and the Mössbauer parameters agree very well with those given for $FeSiO_3$ by Dyar et al. (2013). Very similar conclusions apply to the sample annealed at 900 °C. Again, the signatures of ferrosilite and aegirine are dominant, and a broad sixth doublet can further improve the fit. Its hyperfine parameters are similar to the additional Fe^{3+} component in the amphibole; however, due to severe overlap, its relative area fraction (~7%) is likely to be inaccurate.

Heating in air: Mössbauer spectroscopy

The evolution of the Fe^{3+}/Fe_{tot} ratio in riebeckite heated in air up to 550 °C was described by Oberti et al. (2018) by combining single-crystal structure refinement and Mössbauer spectroscopy. Those data are complemented by the new analyses done on powders annealed at 450, 750, and 800 °C for 8 h (Fig. 4). Based on the data of Oberti et al. (2018), the presence of a significant amount of oxo-amphibole is expected for our experiments after 8 h annealing at 450 °C. Indeed, the Mössbauer spectrum shows a distinct reduction in Fe^{2+} content, especially at the *M*(1) site (~3.2% of total iron, Table 2), while the amount of Fe^{2+} at *M*(3)

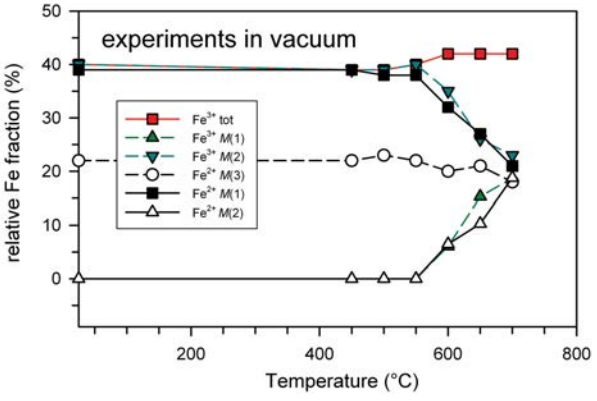

Figure 2. Evolution of the site partitioning of Fe^{3+} and Fe^{2+} in riebeckite annealed in vacuum. (Color online.)

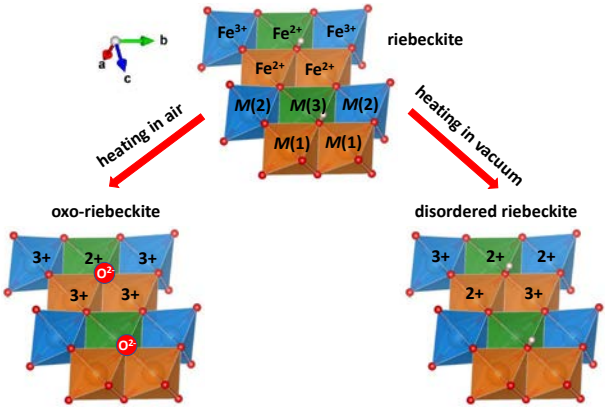

Figure 3. Local structure within the strip of octahedra in amphiboles and schematic representation of the evolution of riebeckite at high *T*. In riebeckite, *M*(2) = 2 Fe^{3+}, *M*(1) = 2 Fe^{2+} and *M*(3) = Fe^{2+} (top); the total charge at the *M*(1,3) sites is 6+ and O(3) = OH. After heating in air, *M*(2) = 2 Fe^{3+}, *M*(1) = 2 Fe^{3+} and *M*(3) = Fe^{2+}, hence the total charge at the *M*(1,3) sites becomes 8+ and O(3) = O^{2-}. After heating in vacuum, the site occupancies are *M*(2) = ($Fe^{3+}Fe^{2+}$), *M*(1) = ($Fe^{3+}Fe^{2+}$), and *M*(3) = Fe^{2+}; the total charge of the *M*(1)*M*(1)*M*(3) triplet is 7+, and local electroneutrality is achieved by changes in the individual bond distances without requiring deprotonation (see text for explanation). Drawing done using Vesta (Momma and Izumi 2008). (Color online.)

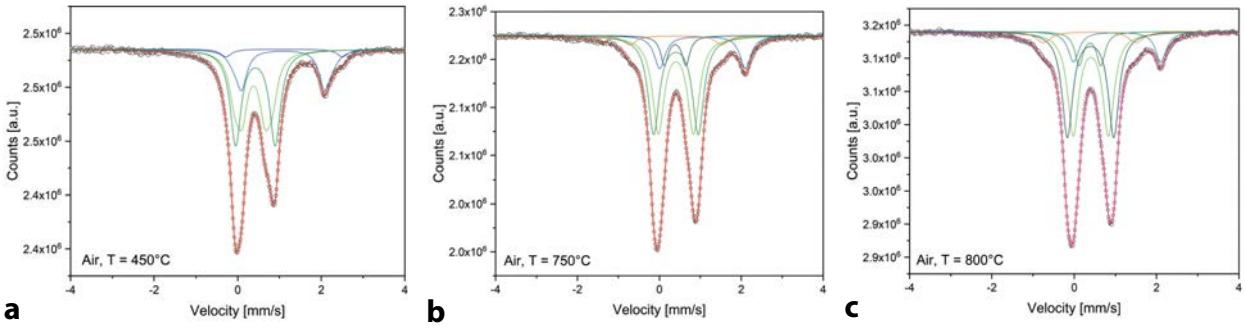

Figure 4. Fitted Mössbauer spectra after annealing the sample in air at different temperatures. (Color online.)

remains almost the same as in the untreated sample. However, the distribution of quadrupole splittings (QSD) was used to model the contribution of $^{M(3)}Fe^{2+}$ because some broadening is observed toward higher QS values with the components centered at 1.987(6) and 2.374(6) mm/s; the average <QS> value is thus given in Table 2. To evaluate the Fe^{3+} resonance absorption correctly, three components are required, and the inner two are assigned to the *M*(2) site as they sum up to 39% of total iron [the value expected for the *M*(2) site], whereas the outer component is assigned to $^{M(1)}Fe^{3+}$. The final fit (Fig. 4) was done using the QSD approach also for $^{M(2)}Fe^{3+}$, where the two components are centered at 0.540(5) and 0.885(5) mm/s at a ratio of 0.55 and 0.45, summing up to the <QS> of 0.689(5).

At 750 and 800 °C, almost all Fe^{2+} is oxidized, and the residual 12% is assigned to the *M*(3) site; we must conclude that at very high temperatures, the *M*(3) site also is involved in the oxidation process, as already observed by Ernst and Wai (1970). The Fe^{2+} contribution in the spectrum can be modeled with one single doublet for Fe^{2+} at *M*(3), but the scenario is far more complex for Fe^{3+}. The broad absorption related to Fe^{3+} might be interpreted based on two doublets plus a small shoulder around +0.65 mm/s. However, two broad shoulders around –0.7 and +1.5 mm/s suggest an additional doublet, the isomer shift of which is typical of ferric iron, whereas the QS is very large (~2.25 mm/s). When using such a three-doublet model, the innermost part of the spectrum, around 0.4 mm/s, cannot be fitted satisfactorily, and the two main Fe^{3+} components have area fractions far from those expected from the stoichiometry of oxo-riebeckite. They are ~15 and ~65% of total iron for the inner and outer doublet, respectively, and the line widths are very different from each other. When introducing a fourth ferric iron component, rapid convergence is obtained, and the two main Fe^{3+} components have similar area fractions and line widths; their area fractions correspond to the expected site populations at the *M*(1) and *M*(3) sites. The newly introduced doublet has a small QS, indicating a rather regular octahedron that is occupied by 7.6% of the total iron; this value, added to the Fe^{2+} refined at the *M*(3) site, sums up rather well to the value expected at this site. In contrast, the broad doublet with the large QS of ~2.25 mm/s can be assigned to ferric iron in a very distorted local environment, as in poorly crystallized iron oxides present as additional phases. At 800 °C, a further small decrease in the $^{M(3)}Fe^{2+}$ content is observed, which scales with the increase of the relative area fraction of the innermost Fe^{3+} doublet, supporting its assignment to $^{M(3)}Fe^{3+}$. The evolution of the Fe^{3+}/Fe^{2+} fractions at the different sites in the full *T* range 300 °C < *T* < 800 °C is shown in Figure 5a, where the data from Oberti et al. (2018), obtained after 3 h annealing, have been combined with the those obtained at higher temperatures (700 and 800 °C, 8 h) during this work.

Table 2. Fitted ^{57}Fe Mössbauer parameters for riebeckite powders annealed in air

Sample ID	IS δ mm/s	QS Δ mm/s	HWHM Γ/2 mm/s	A (%)	Site
450 °C/air	1.113(2)	2.791(7)	0.134(4)	3.2(9)	Fe^{2+} *M*(1)
	1.084(3)	2.064(6)[a]	0.155(4)	19.9(5)	Fe^{2+} *M*(3)
	0.378(2)	0.689(5)[a]	0.153(4)	39.3(6)	Fe^{3+} *M*(2)
	0.423(2)	0.946(6)	0.158(4)	37.6(8)	Fe^{3+} *M*(1)
750 °C/air	1.060(3)	2.087(6)	0.160(3)	12.3	Fe^{2+} *M*(3)
	0.404(1)	0.855(2)	0.171(1)	37.9	Fe^{3+} *M*(2)
	0.404(1)	1.087(2)	0.168(1)	37.9	Fe^{3+} *M*(1)
	0.385(3)	0.522(6)	0.113(2)	7.6	Fe^{3+} *M*(3)
	0.399(1)	2.248(9)	0.192(6)	4.2	Fe^{3+}
800 °C/air	1.045(3)	2.123(6)	0.160(3)	11.0	Fe^{2+} *M*(3)
	0.403(1)	0.854(2)	0.164(1)	37.4	Fe^{3+} *M*(2)
	0.396(1)	1.126(2)	0.157(1)	37.0	Fe^{3+} *M*(1)
	0.381(2)	0.527(4)	0.123(3)	9.1	Fe^{3+} *M*(3)
	0.377(1)	2.255(2)	0.221(2)	5.5	Fe^{3+}

[a] Average QS in the quadrupole splitting distribution (QSD).

The complete transition to oxo-riebeckite at 450 °C (Table 2) is, at first glance, in contrast to the data of Oberti et al. (2018), who noted only partial dehydrogenation at that temperature. However, during this work, we used longer annealing times, which most probably explains the differences in the Fe^{3+} content, as graphically shown in Figure 5b, where the new data at *T* = 450 °C have been added to Figure 5a. Oberti et al. (2018) noted that Fe^{2+} oxidation of starts at the *M*(1) site, and our spectra (Fig. 4) show that a new and very intense $^{M(1)}Fe^{3+}$ contribution with a QS value of 0.946(6) mm/s is indeed present after 8 h annealing at 450 °C. At these conditions, the samples undergo almost complete $^{M(1,2)}Fe^{2+} \rightarrow {}^{M(1,2)}Fe^{3+}$ transformation, the *M*(3) site being virtually unaffected (Table 2). Annealing at higher temperatures shows that about half of the $^{M(3)}Fe^{2+}$ is oxidized at 800 °C; interestingly, the QS values for the doublet used to gain convergence has a lower QS, suggesting that $^{M(3)}Fe^{3+}$ occurs in a more regular octahedral environment. Vice versa, the QS for $^{M(1)}Fe^{3+}$ increases toward 1.126(2) mm/s at 800 °C, indicating a more distorted coordination geometry.

Information from powder X-ray diffraction

The powders annealed in vacuum were examined using X-ray diffraction after each Mössbauer data collection. Phase analysis by the Rietveld method confirms that riebeckite is the only phase

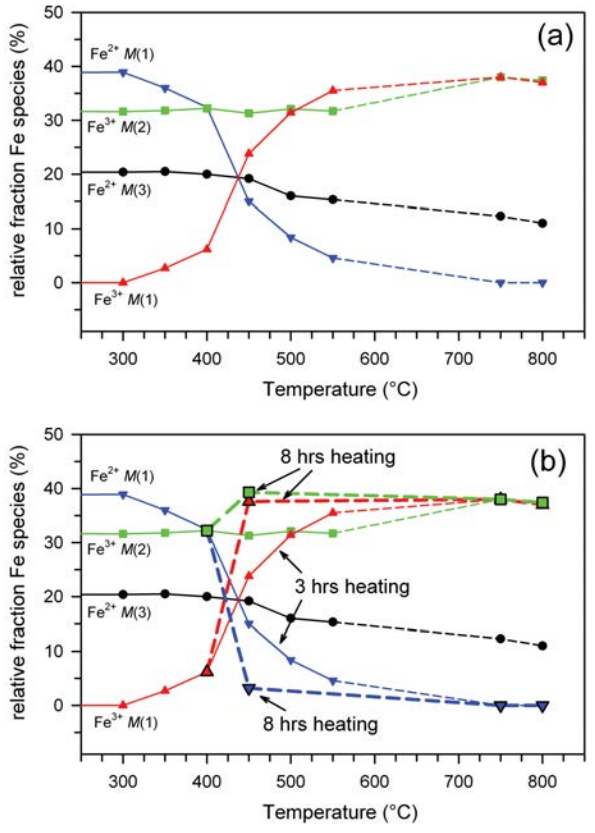

Figure 5. (**a**) Evolution of the Fe speciation and partitioning in riebeckite heated in air as obtained from Mössbauer analysis; data from Oberti et al. (2018) and this work (see text). (**b**) Same diagram as in **a** including the sample annealed at 450 °C for 8 h; the strong difference in the oxidation path obtained with different annealing times is evident. (Color online.)

present up to 700 °C; at 800 °C only minor riebeckite (~20%) is left (Table 3), and most of the sample has transformed into aegirine (ae) + ferrosillite (fs) + cristobalite (cri), according to the (ideal) reaction:

$$\underset{\text{riebeckite}}{2Na_2(Fe^{3+}_2Fe^{2+}_3)Si_8O_{22}(OH)_2} = \underset{\text{aegirine}}{4NaFe^{3+}Si_2O_6} + \underset{\text{ferrosilite}}{6Fe^{2+}SiO_3} + \underset{\text{cristobalite}}{2SiO_2} + \underset{\text{water}}{2H_2O} \quad (2)$$

At 900 °C, no clear evidence of riebeckite is found, and the powder is a mixture of aegirine (67%), ferrosilite (30%), and traces of cristobalite (Table 3). Online Materials[1] Table S1 shows a small decrease in all the unit-cell edges with increasing temperature. A comparison of the lattice parameters refined for aegirine formed during the heating experiment (Online Materials[1] Table S1) with those obtained for phases synthesized along the join hedenbergite (hd) $CaFe^{2+}Si_2O_6$–aegirine (ae) $NaFe^{3+}Si_2O_6$ join (Redhammer et al. 2006), suggests that its chemical composition is close to $Ae_{85}Hd_{15}$. Hence, the minor Ca present in riebeckite (see Oberti et al. 2018) is incorporated into aegirine; note that the presence of Ca in aegirine requires that of an equal amount of Fe^{2+} to obtain electroneutrality (as discussed in the Mössbauer section).

To check for the difference due to the annealing atmosphere, we did a series of quenching experiments in air (8 h) and collected the XRPD patterns ex situ at steps of 50 °C in the 300 °C < T < 900 °C range. The relative phase contents measured in the powder during this second experiment are also shown in Table 3. The XRPD pattern measured after annealing at 400 °C showed a splitting (Fig. 6) of the prominent peak at 28.5° (indexed as 310), and a satisfactory evaluation of the X-ray pattern could only be obtained when using two different sets of parameters, corresponding to riebeckite and oxo-riebeckite, respectively, as structural input data. The same was true for the sample tempered at 425 °C. Quantitative Rietveld analysis indicates that in the sample at 400 °C, the two amphiboles coexist roughly in a 1:1 ratio, while at 425 °C, the ratio is about 35% riebeckite and 65% oxo-riebeckite (Table 3). At 450 °C, the sample is almost only oxo-riebeckite. Increasing the temperature up to 800 °C does not induce any additional change to the XRPD pattern, except for some peak shifts indicative of slight changes in the lattice parameters. At 850 °C, the first evidence for the decomposition of riebeckite was found through the appearance of aegirine and cristobalite, plus small amounts of hematite. At 900 °C, the amphibole disappears, and the run product consists of a mixture of aegirine + hematite + cristobalite. All unit-cell edges (Online Materials[1] Table S1; Fig. 7) decrease abruptly at 400–450 °C; at higher T, there is a gradual decrease up to the breakdown temperature.

The effect of time on the results was preliminarily verified by collecting XRPD data along the 425 °C isotherm at successive intervals of 8 h (Fig. 6). As expected, the peak assigned to riebeckite decreased in intensity as a function of time, and oxidation is nearly complete after 32 h. The unit-cell parameters decrease with prolonged heating but stabilize above 24 h; hence we can assume that after 24 h no significant change occurs in the sample. Based on these tests, we collected XRPD patterns in the 25–35° 2θ range along three isotherms as a function of time.

The structural study on riebeckite powders thermally treated in air was completed by monitoring in situ the evolution of X-ray patterns as a function of temperature. Figure 8a shows that, in the

Table 3. Estimations of phase contents using the Rietveld method (am = amphibole; for other abbreviations see Table 1)

T (°C)	Environment	OH-am	oxo-am	ae	fs	cri	Hem
450	vac	100		–	–	–	–
500	vac	100		–	–	–	–
550	vac	100		–	–	–	–
600	vac	100		–	–	–	–
650	vac	100		–	–	–	–
700	vac	100		–	–	–	–
800	vac	21(4)		50(4)	28(3)	22(1)	–
900	vac	–		67(4)	30(3)	3(1)	–
300	air	100		–	–	–	
400	air	50	50	–	–	–	
425	air	35	65	–	–	–	
450	air	–	100	–	–	–	
500	air	–	100	–	–	–	
600	air	–	100	–	–	–	
700	air	–	100	–	–	–	
800	air	–	100	–	–	–	
850	air	–	49(2)	39(2)	–	9(1)	3(1)
900	air	–	–	58(2)	–	24(1)	18(1)

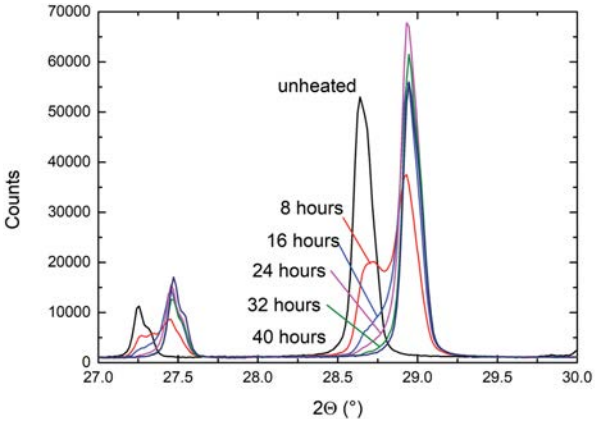

Figure 6. Evolution of the (310) peak splitting for riebeckite annealed at constant $T = 425$ °C as a function of time. X-ray patterns were collected at room temperature (see text for explanation). (Color online.)

R$T < T < 400$ °C range, the positions of the diffraction peaks shift gradually as a consequence of the thermal expansion of the unit cell. Between 425 and 450 °C, there is an abrupt change in the patterns: the (201) and (310) diffraction peaks are, in fact, suddenly displaced toward higher 2θ values. Such shift is compatible with a major contraction of the unit-cell parameters. The unit-cell dimensions measured at increasing T values are listed in Online Materials[1] Table S2; the evolution of the unit-cell volume is shown in Figure 8b. According to Oberti et al. (2018), during the heating cycle (filled squares), the gradual increase in all the unit-cell dimensions up to 425 °C is due to the thermal expansion of the structure. From 425 to 450 °C, there is a decrease in all the parameters. Above 450 °C thermal expansion occurs and has the same slope as in the first part of the experiment; analysis of the patterns shows the presence of oxo-riebeckite alone, at least up to 800 °C. During the cooling cycle (dotted squares in Fig. 8b), the unit-cell volume of oxo-riebeckite decreases linearly.

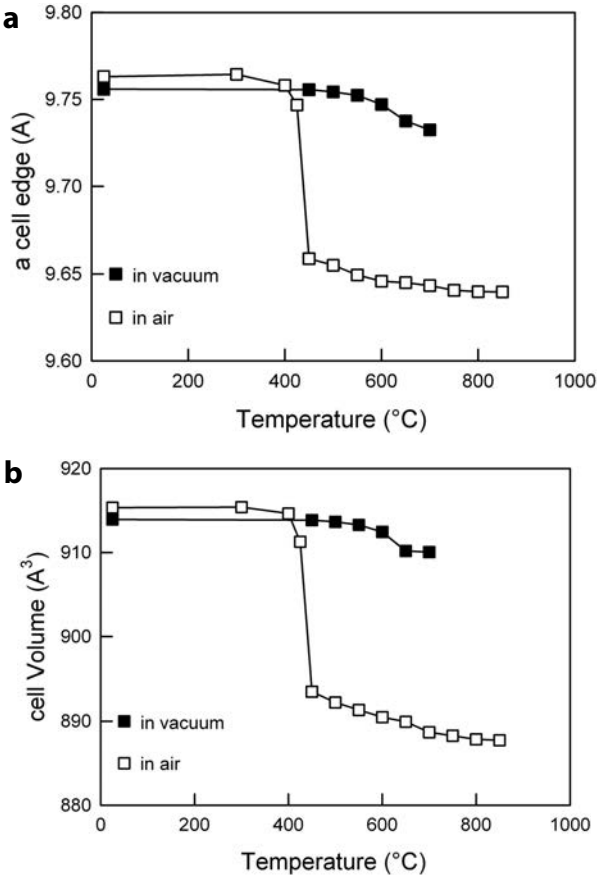

Figure 7. The evolution of the unit-cell volume and the *a* cell-edge observed in riebeckite when heated in vacuum vs. in air.

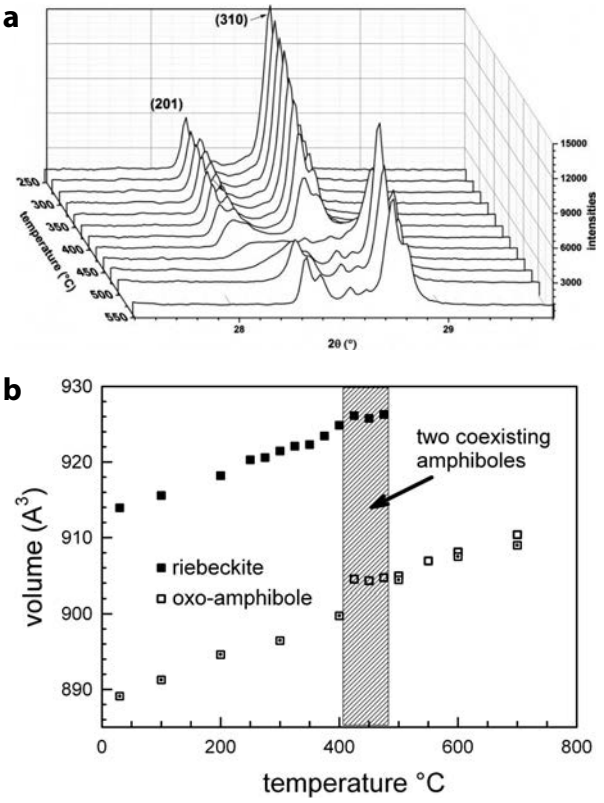

Figure 8. (**a**) Evolution of the XRPD pattern of riebeckite collected in situ in the 27–30° 2θ range as a function of temperature. (**b**) Evolution of the unit-cell volume measured for riebeckite powders heated in air; data collected in situ. The dotted empty squares were collected during cooling.

The kinetics of the riebeckite to oxo-riebeckite transition

Both the Mössbauer and the XRPD data discussed above show that in air the riebeckite to oxo-riebeckite transition occurs in the 400–450 °C temperature range, where both phases coexist (Figs. 6 and 8).

Della Ventura et al. (2021) addressed the kinetics of riebeckite dehydrogenation by using FTIR spectroscopy and showed that H loss in powdered riebeckite can be modeled as a first-order reaction. In this work, we studied the same transition by monitoring the intensity of the (310) diffraction peak (Fig. 6) at 400, 425, and 450 °C as a function of time.

A general discussion on the different approaches to kinetics

is found in Hancock and Sharp (1972) or in Brown et al. (1980). For amphibole powders, the dehydrogenation process can be conveniently treated by using the Avrami-Erofeev equation that can be expressed as:

$$y = 1 - \exp[-f(t)] \text{ or } I_R = I_{sum} \cdot \exp[-f(t)] \quad (3)$$

where $y = 1 - I_R/I_{sum}$ is the fraction of oxo-riebeckite at time = t (min), I_R is the intensity of the (310) peak of riebeckite at time = t, I_{sum} is the sum the intensities of the (310) peaks of riebeckite and oxo-riebeckite at time = t; $f(t)$ is an exponential function (Avrami 1939). Della Ventura et al. (2021) used a slightly different equation:

$$I_R = I_{sum} \cdot \exp[-(k \cdot t)^m] \quad (4)$$

where the exponential function $f(t)$ is described by two parameters k and m. The coefficient k, the rate constant, describes the decreasing trajectory vs. the concentration of the reactant, while the exponential factor m is an empirical factor used to model the reaction mechanism; m close to 1.0 indicates first-order reactions (Hancock and Sharp 1972).

An example of fitting this equation to our experimental XRPD data is given in Figure 9a, and the resulting parameters are listed in Table 4. The temperature dependence of the rate constant, k, as expressed by the Arrhenius Equation 4, can be used to calculate the activation energy E_a (kJ/mol) for the transition from riebeckite to oxo-riebeckite:

$$k = A \cdot \exp\left(-\frac{E_a}{RT}\right) \quad (5)$$

where R is the universal gas constant (J/mol), T is the temperature in Kelvin, and A is the pre-exponential factor. In this equation, the activation energy represents the limiting energy barrier for the reaction to proceed, while the pre-exponential factor is the reaction frequency (Galwey and Brown 1999). The rate constants k from Table 4 are plotted in the Arrhenius space (Fig. 9b) and the activation energy (E_a) is given by the slope of the regression line across the data points multiplied by R (the gas constant). In Figure 9b, the k values obtained during this work by monitoring the (310) peak in the XRPD patterns align with those obtained for riebeckite powders studied via FTIR spectroscopy by Della Ventura et al. (2021). Figure 9b thus shows that probing the same phenomenon from two distinct points of view, i.e., the structure adjustment due to the Fe oxidation (XRPD) and the loss of H^+ (FTIR), indicates that the two processes have the same energetics. The calculated E_a for the riebeckite to oxo-riebeckite transition using all data plotted in Figure 9b is 166 ± 6 kJ/mol.

Table 4. Fitting parameters obtained using the Avrami equation for the isothermal experiment on riebeckite powders

Temperature (°C)	k	*m*	–log k
450	0.0100 (5)	1.18 (7)	4.61 (3)
425	0.00317 (6)	0.82 (2)	5.75 (1)
400	0.00151 (5)	1.09 (5)	6.50 (2)

Notes: The uncertainty on the last digit is given in parentheses.

Discussion

Riebeckite is a common rock-forming mineral under high-pressure metamorphic conditions (Deer et al. 1997) and has been the main asbestos mineral used in a large variety of technological applications for at least one century (Gunther et al. 2007).

The crystal chemistry of the amphiboles is controlled by a complex interconnection between the chemistry of the geological system (be it a rock subject to metamorphism or a melt) and the P-T-f_{O_2/H_2O} conditions (see Martin 2007 and Schumacher 2007). The main crystal-chemical response to changes in boundary conditions is the loss of H^+ (dehydrogenation); accordingly, the first criterion presently used for classification in the amphibole supergroup is the relative amount of the W anions (OH^-,O^{2-}) in the general formula (Hawthorne et al. 2012).

There are two mechanisms controlling the OH^- content of the amphiboles:

(1) Crystallization in the presence of ^{C}Ti (Oberti et al. 1992, 2015; Della Ventura et al. 2007; Gatta et al. 2017; Liao et al. 2021); this feature is well known in amphiboles from mantle-related occurrences where the compositions are typically ^{C}Ti-rich and OH^- poor (Dyar et al. 1993).

(2) Oxidation of Fe according to Equation 1 when T increases, for example, during subduction.

Significant efforts have been made toward understanding how much the OH^-/O^{2-} ratio in amphiboles is affected by the redox state of the mantle source and how much it is due to post-crystallization events, such as reactions during magma uplift to

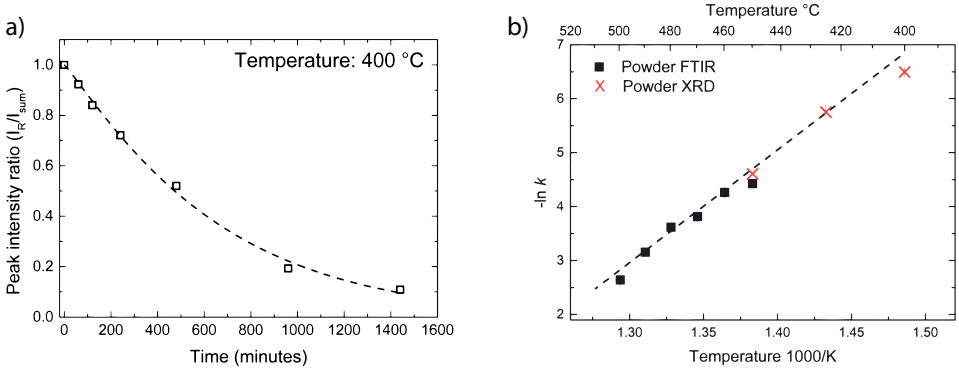

Figure 9. (**a**) Normalized integrated peak ratio (I_R/I_{sum}) as a function of time during the isothermal 400 °C experiments on riebeckite powder. The dashed line is the fitted the Avrami-Erofeev equation. (**b**) Arrhenius plot for the kinetic data measured both via FTIR (squares, from Della Ventura et al. 2021) and XRD (stars, this work). Error bars are smaller than the symbols. (Color online.)

the surface and post-effusive oxidation (Dyar et al. 1993). An intriguing feature already observed in early experiments (Popp et al. 2006) and demonstrated by recent work (Della Ventura et al. 2018; Mihailova et al. 2021) is that Equation 1 is reversible in a relatively broad range of temperatures; this is indeed an issue that has several implications, both in Geology and Geophysics and in Material Science.

The results of this work clearly show that the riebeckite may follow two totally different thermodynamic paths as a function of temperature. At oxidizing conditions, it is stable in the hydrous form up to relatively low temperatures; it undergoes a sudden transformation to oxo-riebeckite, which is completed within ~50 °C, and then is stable up to high-T [~800 °C for powders, this work and ~900 °C for single-crystals (Oberti et al. 2018)]. X-ray diffraction shows a reduction of the unit-cell parameters in the 400–450 °C range (Figs. 7 and 8), with a significant contraction of the octahedra where Fe^{2+} oxidizes to Fe^{3+} (ionic radii: Fe^{2+} = 0.78 Å and Fe^{3+} = 0.645 Å, respectively, Shannon 1976) coupled with a simultaneous loss of H^+ to maintain local electroneutrality. These structural modifications cause a major decrease of the a edge-length (which is particularly sensitive to H^+ loss, see for example, Robert et al. 1989) and of the b edge-length (which is particularly sensitive to the dimension of the octahedra, e.g., Colville et al. 1966).

The rate constants (k) measured at different temperatures for the riebeckite to oxo-riebeckite transition at oxidizing conditions align (Fig. 9b) with those measured via FTIR by Della Ventura et al. (2021); this implies that the two techniques probe different aspects of the same process and are strongly correlated. However, Figure 10 shows that the structural adjustment is virtually complete at 450 °C, whereas dehydrogenation needs higher temperatures to be effective. This is in agreement with the observation of Della Ventura et al. (2018, 2021) and Mihailova et al. (2021) that the electronic transfer precedes and triggers the structural modifications and the final loss of H. The activation energy for dehydrogenation in riebeckite is in agreement with previous data from the literature (Clark and Freeman 1967; Della Ventura et al. 2021).

According to Equation 1, this transformation is strongly dependent upon the availability of external oxygen and, when this is the case, may lead to the release of water into the surrounding system. For this reason, Fe-amphiboles are considered among the main carriers of water in the lower crust and upper mantle. Note that in this process, the amphibole provides H^+ and not water to the system (Hu et al. 2018; Mihailova et al. 2021). The final breakdown products of the oxo-amphibole include aegirine + cristobalite + hematite. At 900 °C, the transformation is virtually complete (Table 3).

Under vacuum, there is almost no Fe oxidation, and riebeckite is stable as a hydrous amphibole up to 700–750 °C; in the XRPD patterns, there is no evidence of transformation into an oxo-amphibole (i.e., no peak splitting, see above). However, in the 550 < T < 700 °C range, riebeckite undergoes a significant cationic re-arrangement to $^{C}R^{3+}$ disordered riebeckite that, at 800 °C, decomposes into aegirine + fayalite + cristobalite + H_2O. This scenario is clarified by the evolution of the Fe speciation and partitioning in riebeckite as a function of T provided by Mössbauer spectroscopy and summarized in Figure 10, where

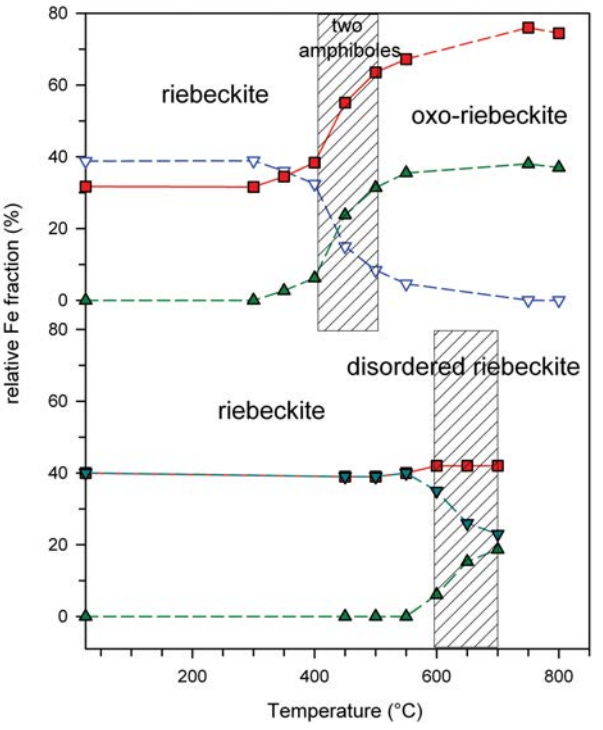

Figure 10. Evolution of the Fe^{3+}/Fe^{2+} site occupancies (from Mössbauer data) in riebeckite annealed in air [data from Oberti et al. (2018); combined with those from this work] vs. the Fe^{3+}/Fe^{2+} site occupancies annealed in vacuum. (Color online.)

the stability ranges of riebeckite and $^{C}R^{3+}$ disordered riebeckite are shown. Oberti et al. (2018) found that the oxo-amphibole obtained by heating riebeckite in air had significant ^{A}Na, in agreement with experimental work showing that sodium amphiboles in high-T in oxidizing conditions deviate in composition toward arfvedsonite (Ernst 1962, 1968). Under reducing conditions, such disorder does not occur. This study was done on powders, and hence we could not refine ^{A}Na occupancy in the resulting amphiboles. However, we note that any migration of Na from the M(4) to the A site should imply migration of $^{C}Fe^{2+}$ to M(4), and Mössbauer spectroscopy shows that this is not the case.

Implications

The first geological implication of our work is that under reducing conditions, the stability limit of riebeckite (structurally speaking) is at least 100 °C lower than under oxidizing conditions. Reducing conditions, on the other side, may stabilize the pyroxene phase(s) and promote riebeckite breakdown.

The second important implication is that characterization of the overall oxidation state of iron does not necessarily provide the oxidation state of the environment of formation because $^{C}R^{3+}$ disordered riebeckite is stable under reducing conditions and has the same Fe^{3+}/Fe^{2+} ratio of riebeckite. Therefore, a possible correlation between the oxidation state of the amphibole and the temperature, for any petrological reconstruction, must necessarily take into consideration the cation site distribution (i.e., the crystal chemistry) as well as the Fe^{3+}/Fe^{2+} ratio (i.e.,

the chemical composition) of the sample.

Regarding possible geophysical implications, this study shows that the different stability of OH-amphiboles vs. oxo-amphiboles must be taken into account when interpreting and extrapolating the conductivity data and the connection between polaron vs. ionic (fluid-mediated) conductivity (Hu et al. 2018).

Finally, the possible role of pressure in the HT processes involving Fe-amphiboles and its consequences on oxidation/conduction has not been addressed during this work, and data in the literature are extremely scarce. The early work of Ernst (1962, 1968) suggests that the role of pressure on the stability of riebeckites is negligible; however, our data definitively suggest that experimental studies aimed at clarifying the actual effect of pressure on the hydroxy-oxo transition in riebeckite and more generally in amphiboles are highly desirable. In this context, it is worth considering the work of Burns et al. (1972), who studied via Mössbauer spectroscopy the pressure-induced change in the oxidation state of iron in a synthetic (Mg,Fe)-riebeckite. With increasing *P*, they observed a significant reduction of Fe^{3+} to Fe^{2+} in the sample; fitting of the Mössbauer spectra showed that Fe reduction occurred mainly at *M*(3) up to 20 kbar and at *M*(1) for higher pressures. This result, which is not yet definitively clarified, further strengthens the connection between the role of the hydrogen bonded to O(3) in maintaining the local electroneutrality during iron oxidation/reduction.

Acknowledgments and Funding

We thank Gerold Tippelt (Salzburg) for help with Mössbauer data collection and Thomas Schwab (Salzburg) for the annealing experiments. Financial support was provided by the Grant to Department of Science, Roma Tre University (MIUR-Italy Dipartimenti di Eccellenza, ARTICOLO 1, COMMI 314-337 LEGGE 232/2016). The final version of the work benefited from positive criticism by F.C. Hawthorne (Winnipeg, Manitoba) and an anonymous referee.

References cited

Addison, W.E., and Sharp, J.H. (1962) Amphiboles. Part III. The reduction of crocidolite. Journal of the Chemical Society (Resumed), 3693–3698.

Addison, W.E., Neal, G.H., and Sharp, J.H. (1962) Amphiboles. Part II. The kinetics of oxidation of crocidolite. Journal of the Chemical Society (Resumed), 1472–1475.

Avrami, M. (1939) Kinetics of phase change. I. General theory. The Journal of Chemical Physics, 7, 1103–1112.

Brown, M.E., Dollimore, D., and Galwey, A.K. (1980) Reactions in the Solid State. Elsevier.

Burns, R.G., Tossell, J.A., and Vaughan, D.J. (1972) Pressure-induced reduction of a ferric amphibole. Nature, 240, 33–35.

Clark, M.W., and Freeman, A.G. (1967) Kinetics and mechanism of dihydroxylation of crocidolite. Transactions of the Faraday Society, 63, 2051–2056.

Colville, P.A., Ernst, W.G., and Gilbert, M.C. (1966) Relationships between cell parameters and chemical compositions of monoclinic amphiboles. American Mineralogist, 51, 1727–1754.

Deer, W.A., Howie, R.A., and Zussman, J. (1997) Double-Chain Silicates, 2nd ed., p. 764. The Geological Society.

Della Ventura, G., Hawthorne, F.C., Robert, J.-L., Delbove, F., Welch, M.D., and Raudsepp, M. (1999) Short-range order of cations in synthetic amphiboles along the richterite–pargasite join. European Journal of Mineralogy, 11, 79–94.

Della Ventura, G., Hawthorne, F.C., Robert, J.-L., and Iezzi, G. (2003) Synthesis and infrared spectroscopy of amphiboles along the tremolite–pargasite join. European Journal of Mineralogy, 15, 341–347.

Della Ventura, G., Oberti, R., Hawthorne, F.C., and Bellatreccia, F. (2007) Single-crystal FTIR study Ti-rich pargasites from Lherz: The spectroscopic detection of $^{O3}O^{2-}$ in amphiboles. American Mineralogist, 92, 1645–1651.

Della Ventura, G., Redhammer, G., Robert, J.L., Sergent, J., Iezzi, G., and Cavallo, A. (2016) Crystal-chemistry of synthetic amphiboles along the join richterite—ferro-richterite: A combined spectroscopic (FTIR, Mössbauer), XRPD and microchemical study. Canadian Mineralogist, 54, 97–114.

Della Ventura, G., Mihailova, B., Susta, U., Cestelli Guidi, M., Marcelli, A., Schlüter, J., and Oberti, R. (2018) The dynamics of Fe oxydation in riebeckite: A model for amphiboles. American Mineralogist, 103, 1103–1111.

Della Ventura, G., Radica, F., Galdenzi, F., Susta, U., Cinque, G., Mihailova, B., and Marcelli, A. (2021) Kinetics of hydrogen diffusion in riebeckite, $Na_2Fe_2^{3+}Fe_3^{2+}Si_8O_{22}(OH)_2$: An HT-FTIR study. American Mineralogist, 107, 754–764.

Dyar, M.D., Macwell, S.J., McGuire, A.V., Cross, L.R., and Robertson, J.D. (1993) Crystal chemistry of Fe^{3+} and H^+ in mantle kaersutites: implications for mantle metasomatism. American Mineralogist, 78, 968–979.

Dyar, M.D., Klima, R.L., Fleagle, A., and Peel, S.E. (2013) Fundamental Mössbauer parameters of synthetic Ca-Mg-Fe pyroxenes. American Mineralogist, 98, 1172–1186.

Ernst, W.G. (1962) Synthesis and stability relations and occurrence of riebeckite and riebeckite-arfvedsonite solid solutions. The Journal of Geology, 70, 689–636.

——— (1968) Amphiboles, 125 p. Springer-Verlag.

Ernst, W.G., and Wai, M. (1970) Mössbauer, infrared, X-ray and optical study of cation ordering and dehydrogenation in natural and heat-treated sodic amphiboles. American Mineralogist, 55, 1226–1258.

Galdenzi, F., Della Ventura, G., Cibin, G., Macis, S., and Marcelli, A. (2018) Accurate Fe^{3+}/Fe^{tot} ratio from XAS spectra at the Fe K-edge. Radiation Physics and Chemistry, 175, 108088. doi.org/10.1016/J.radphyschem.2018.12.008.

Galwey, A.K., and Brown, M.E. (1999) Thermal Decomposition of Ionic Solids, 596 p. Elsevier.

Gatta, G.D., McIntyre, G.J., Oberti, R., and Hawthorne, F.C. (2017) Order of $^{[6]}Ti^{4+}$ in a Ti-rich calcium amphibole from Kaersut, Greenland: A combined X-ray and neutron diffraction study. Physics and Chemistry of Minerals, 44, 83–94.

Gunther, M.E., Belluso, E., and Mottana, A. (2007) Amphiboles: Environmental and health concerns. In F.C. Hawthorne, R. Oberti, G. Della Ventura, and A. Mottana, Eds., Amphiboles: Crystal Chemistry, Occurrence and Health Issues, 67, 453–516. Reviews in Mineralogy and Geochemistry, Mineralogical Society of America, Chantilly, Virginia.

Hancock, J.D., and Sharp, J.H. (1972) Method of comparing solid-state kinetic data and its application to the decomposition of kaolinite, brucite, and $BaCO_3$. Journal of the American Ceramic Society, 55, 74–77.

Hawthorne, F.C., and Della Ventura, G. (2007) Short-range order in amphiboles. In F.C. Hawthorne, R. Oberti, G. Della Ventura, and A. Mottana, Eds., Amphiboles: Crystal Chemistry, Occurrence and Health Issues, 67, 173–222. Reviews in Mineralogy and Geochemistry, Mineralogical Society of America, Chantilly, Virginia.

Hawthorne, F.C., and Oberti, R. (2007) Amphiboles: Crystal chemistry. In F.C. Hawthorne, R. Oberti, G. Della Ventura, and A. Mottana, Eds., Amphiboles: Crystal Chemistry, Occurrence and Health Issues, 67, 1–54. Reviews in Mineralogy and Geochemistry, Mineralogical Society of America, Chantilly, Virginia.

Hawthorne, F.C., Oberti, R., Harlow, G.E., Maresch, W.V., Martin, R.F., Schumacher, J.C., and Welch, M.D. (2012) Nomenclature of the amphibole supergroup. American Mineralogist, 97, 2031–2048.

Hodgson, A.A., Freeman, A.G., and Taylor, H.F.V. (1965) The thermal decomposition of crocidolite from Koegas. South Africa. Mineralogical Magazine, 35, 5–29.

Hu, H., Dai, L., Li, H., Sun, W., and Li, B. (2018) Effect of dehydrogenation on the electrical conductivity of Fe-bearing amphibole: Implications for high conductivity anomalies in subduction zones and continental crust. Earth and Planetary Science Letters, 498, 27–37.

Larson, A.C., and Von Dreele, R.B. (2000) General Structure Analysis System (GSAS). Los Alamos National Laboratory Report LAUR 86-748.

Liao, Y., Wei, C., and Rehman, H.U. (2021) Titanium in calcic amphibole: behaviour and thermometry. American Mineralogist, 106, 180–191.

Martin, R.F. (2007) Amphiboles in the igneous environment. In F.C. Hawthorne, R. Oberti, G. Della Ventura, and A. Mottana, Eds., Amphiboles: Crystal Chemistry, Occurrence and Health Issues, 67, 325–358. Reviews in Mineralogy and Geochemistry, Mineralogical Society of America, Chantilly, Virginia.

Mihailova, B., Della Ventura, G., Waselmann, N., Xu, W., Schluter, J., Galdenzi, F., Marcelli, A., Redhammer, G.J., Boiocchi, M., and Oberti, R. (2021) Coupled phonon-electron excitations in hydrous Fe-bearing silicates: A key to understanding lithospheric conductivity. Communication Materials, 2, 57. doi.org/10.1038/s43246-021-00161-y

Momma, K., and Izumi, F. (2008) VESTA: a three-dimensional visulization system for electronic and structural analysis. Journal of Applied Crystallography, 41, 653–658.

Oberti, R., Ungaretti, L., Cannillo, E., and Hawthorne, F.C. (1992) The behaviour of Ti in amphiboles. Four - and six-coordinate Ti in richterite. European Journal of Mineralogy, 4, 425–440.

Oberti, R., Hawthorne, F.C., Ungaretti, L., and Cannillo, E. (1995) $^{[6]}$Al disorder in amphiboles from mantle peridotite. Canadian Mineralogist, 33, 867–878.

Oberti, R., Boiocchi, M., Hawthorne, F.C., Cámara, F., Ciriotti, M., and Berge, S.A. (2015) Ti-rich fluoro-richterite from Kariåsen (Norway): The oxo-component and the use of Ti^{4+} as a proxy. Canadian Mineralogist , 53, 285–294.

Oberti, R., Boiocchi, M., Zema, M., Hawthorne, F.C., Redhammer, G.J., Susta, U., and Della Ventura, G. (2018) Understanding the peculiar H*T* behavior of riebeckite: espansivity, deprotonation, Fe-oxidation and a novel cation disorder

scheme. European Journal of Mineralogy, 30, 437–449.
Popp, R.K., Hibbert, H.A., and Lamb, W.M. (2006) Oxy-amphibole equilibria in Ti-bearing calcic amphiboles: Experimental investigation and petrologic implications for mantle-derived amphiboles. American Mineralogist, 91, 54–66.
Rancourt, D.G., and Ping, J.Y. (1991) Voigt-based methods for arbitrary-shape static hyperfine parameter distributions in Mössbauer spectroscopy. Nuclear Instruments and Methods in Physics Research Section B: Beam Interactions with Materials and Atoms, 58, 85–97.
Rancourt, D.G., McDonald, A.M., Lalonde, A.E., and Ping, J.Y. (1993) Mössbauer absorber thickness for accurate site populations in Fe-bearing minerals. American Mineralogist, 78, 1–7.
Rancourt, D.G., Ping, J.Y., Boukili, B., and Robert, J.-L. (1996) Octahedral-site Fe^{2+} quadrupole splitting distributions from Mössbauer spectroscopy along (OH, F)-annite join. Physics and Chemistry of Minerals, 23, 63–71.
Redhammer, G.J., Amthauer, G., Roth, G., Tippelt, G., and Lottermoser, W. (2006) Single-crystal X-ray diffraction and temperature dependent ^{57}Fe Mossbauer spectroscopy on the hedenbergite-aegirine $(Ca,Na)(Fe^{2+},Fe^{3+})Si_2O_6$ solid solution. American Mineralogist, 91, 1271–1292.
Robert, J.-L., Della Ventura, G., and Thauvin, J.-L. (1989) The infrared OH-stretching region of synthetic richterites in the system Na_2O-K_2O-CaO-MgO-SiO_2-H_2O-HF. European Journal of Mineralogy, 1, 203–211.
Shannon, R.D. (1976) Revised effective ionic radii and systematic studies of interatomic distances in halides and chalcogenides. Acta Crystallographica, A32, 751–767.
Schumacher, J.C. (2007) Metamorphic amphiboles: composition and coexistence In F.C. Hawthorne, R. Oberti, G. Della Ventura, and A. Mottana, Eds., Amphiboles: Crystal Chemistry, Occurrence and Health Issues, 67, 359−416. Reviews in Mineralogy and Geochemistry, Mineralogical Society of America, Chantilly, Virginia.
Susta, U., Della Ventura, G., Hawthorne, F.C., Abdu, Y.A., Day, M.C., Mihailova, B., and Oberti, R. (2018) The crystal-chemistry of riebeckite, ideally $Na_2Fe_3^{2+}Fe_2^{3+}Si_8O_{22}(OH)_2$: A multi-technic study. Mineralogical Magazine, 82, 837–852.
Whitfield, H.J., and Freeman, A.G. (1967) Mössbauer study of amphiboles. Journal of Inorganic and Nuclear Chemistry, 29, 903–914.

Manuscript received March 26, 2021
Manuscript accepted December 3, 2021
Accepted manuscript online December 20, 2021
Manuscript handled by Maarten A.T.M. Broekmans

Endnote:

[1]Deposit item AM-23-18073, Online Materials. Deposit items are free to all readers and found on the MSA website, via the specific issue's Table of Contents (go to http://www.minsocam.org/MSA/AmMin/TOC/2023/Jan2023_data/Jan2023_data.html).